

KeyNode-Driven Geometry Coding for Real-World Scanned Human Dynamic Mesh Compression

Huong Hoang, Truong Nguyen, *Fellow*, IEEE, and Pamela Cosman, *Fellow*, IEEE

Abstract—The compression of real-world scanned 3D human dynamic meshes is an emerging research area, driven by applications such as telepresence, virtual reality, and 3D digital streaming. Unlike synthesized dynamic meshes with fixed topology, scanned dynamic meshes often not only have varying topology across frames but also scan defects such as holes and outliers, increasing the complexity of prediction and compression. Additionally, human meshes often combine rigid and non-rigid motions, making accurate prediction and encoding significantly more difficult compared to objects that exhibit purely rigid motion. To address these challenges, we propose a compression method designed for real-world scanned human dynamic meshes, leveraging embedded key nodes. The temporal motion of each vertex is formulated as a distance-weighted combination of transformations from neighboring key nodes, requiring the transmission of solely the key nodes’ transformations. To enhance the quality of the KeyNode-driven prediction, we introduce an octree-based residual coding scheme and a Dual-direction prediction mode, which uses I-frames from both directions. Extensive experiments demonstrate that our method achieves significant improvements over the state-of-the-art, with an average bitrate saving of 24.51% across the evaluated sequences, particularly excelling at low bitrates.

Index Terms—Dynamic Mesh Compression, 3D Human Dynamic Mesh, Varying Topology

I. INTRODUCTION

The inherent depth and multitude of viewing angles enabled by 3D dynamic meshes contribute to an enriched experience across various applications, such as telepresence, virtual reality, and 3D digital streaming. Scanned 3D human dynamic meshes hold particular significance. They enable realistic representation and sharing of human motion, a capability increasingly accessible due to advancements in affordable scanning technologies. This accessibility is driving broader adoption, from entertainment and training simulations to healthcare and communication. However, the vast storage and transmission demands of these data-rich meshes necessitate efficient compression techniques designed to preserve the structural integrity and motion fidelity of scanned human meshes.

Unlike synthesized dynamic meshes, such as those created using graphic design software, which typically feature fixed topology and well-defined structures, real-world scanned human meshes present unique challenges. Their topology often varies across frames, with changes in the number, connectivity, and correspondence of vertices. Furthermore, scanned meshes frequently suffer from defects such as holes, noise, and outliers, adding complexity to both prediction and compression.

This work was supported by the Center for Wireless Communications, University of California, San Diego, and by the National Science Foundation under Grant DUE-1928604.

Developing methods that can effectively account for this temporal and spatial variability is a critical research challenge.

Human meshes also introduce challenges due to the combination of rigid motion (often for arms and legs) and non-rigid motion (often for the torso, fingers, and clothing). Unlike rigid objects, human motion involves intricate deformations and fine-grained movements that demand more sophisticated modeling to achieve accurate prediction and efficient compression.

This paper builds on our previous work [1], where we introduced a *KeyNode-based* approach to describe the motion of evolving meshes using strategically placed key nodes. While our earlier research demonstrated the potential of using sparse key nodes to capture temporal motion in real-world scanned dynamic human meshes, this paper significantly extends the framework with new techniques that enhance both compression efficiency and temporal prediction. Specifically, we achieve better compression rates by explicitly quantizing KeyNode-driven motion vectors and optimizing entropy coding through the transfer of Huffman dictionaries fitted to Cauchy distributions. Moreover, we propose Octree-based residual coding to enhance geometry prediction accuracy and introduce a Dual-Direction prediction mode, enabling more adaptable modeling of dynamic human motion over time.

Taken together with our prior contributions, these new advancements result in a comprehensive framework that effectively addresses the key challenges of compressing scanned 3D human dynamic meshes. Our codec offers the following key contributions:

- **Tackling Topology Variability:** Instead of calculating the motion vector of individual vertices, which can be highly sensitive to changes in topology and scan defects, our method uses the motion of sparse controlling keynodes to represent vertex movement. This approach effectively captures the dynamics of the mesh, even with varying topology.
- **Efficient Handling of Human Motion:** To compute the KeyNode-driven motion vectors, the KeyNode-Driven Codec uses a hybrid registration model that combines embedded and isometric deformation, capturing effectively both the rigid and non-rigid complexities of human motion, ensuring fidelity for intricate deformations in both anatomy and clothing.
- **Effective Temporal Prediction Enhancement:** We propose Octree-based residual coding and a Dual-Direction prediction mode to effectively address prediction errors and better capture the complexities of dynamic human motion over time.

Overall, our codec effectively addresses the challenges inherent in compressing real-world scanned 3D human dynamic meshes, including topology variability and complex human motion. The experimental results show that our method significantly outperforms the state-of-the-art codec, particularly at low bitrates.

The remainder of this paper is organized as follows. Section II reviews related work on scanned dynamic mesh compression. Section III introduces our proposed codec, detailing the KeyNode-Driven compression framework, Octree-based residual coding, and Dual-direction prediction. Section IV presents the experimental setup and results. Finally, Section V concludes the paper and outlines future work.

II. RELATED WORK

In this section, we review dynamic mesh compression methods. Methods designed for meshes with fixed topology, where vertex correspondences are available across frames, rely on the topology remaining constant, allowing for predictable encoding of vertex motion [2]–[12]. For real-world scanned dynamic meshes, where the topology can change, and vertex correspondences are not inherently available, compression methods must accurately capture the temporal variations without explicit vertex correspondence. Previous methods can be organized into distinct categories.

Re-meshing-based methods: Mesh frames with inconsistent topology can be mapped onto a uniform topology by re-meshing. In [13], an approximate global topology for the whole mesh sequence was constructed by re-meshing the first frame and mapping it to the following frames using motion estimation. Similarly, [14] employs separate Groups of Frames (GoFs), with each GoF having its own global topology.

Block matching-based methods: Extending 2D video block matching, the method proposed in [15] estimates temporal motion by block-wise comparisons. The 3D model is divided into block-based surfaces using cubic blocks, and their motions are estimated by searching for the best match block in the reference mesh frame. Similarly, a patch-based matching algorithm [16] involves dividing frames into patches of the same surface area. For a patch in the current frame, the reference patch is determined as the one in the reference frame with the minimum dissimilarity.

Video-based methods: The Visual Volumetric Video-based Coding (V3C) standard is used in [17] to encode meshes with orthogonal projections, followed by atlas packing and video coding. Numerous proposals employing video-based methods were put forward in response to MPEG’s CfP for Dynamic Mesh Compression [18]. MPEG’s benchmark codec, known as Anchor, involves initial geometry encoding of each frame with mesh decimation and Draco compression [19]. Texture frames are stacked into a video and encoded with standard video coding techniques. A patch-based approach was presented in [20] reorganizing the intra-frame and inter-frame texture tiles to improve spatial and temporal correlation. In addition to mesh decimation, Mammou et al. proposed incorporating mesh subdivision, producing a base mesh and a series of subdivided meshes linked to their respective displacement vectors [21].

The displacements undergo wavelet transform, followed by quantization and packing into a 2D image or video, which is encoded by an image/video compression technique. MPEG adopted this approach [21] for further development into a new standard, named Video-based Dynamic Mesh Coding (V-DMC). Following its establishment, various efforts have been made to enhance V-DMC [22]–[31].

III. PROPOSED CODEC

To address the challenge of inconsistent topology, which eliminates the need for explicit vertex correspondence, our KeyNode-Driven Compression method, originally introduced in [1], leverages embedded key nodes to represent motion vectors while ensuring efficient compression. The temporal motion of each vertex is formulated as a distance-weighted combination of transformations from its neighboring key nodes. The process is depicted in Fig. 1. Starting with the geometry of frame $t - 1$, we use the embedded key nodes to predict the geometry of frame t through embedded deformation, where the geometry of frame $t - 1$ is deformed to estimate the geometry of frame t . Since keynodes are typically sparse and the motion vectors are quantized, prediction errors arise. To address these, we employ Octree-based residual coding to refine the predicted geometry for frame t . At the sequence level, we enhance the prediction process with a Dual-direction prediction mode. The details of the KeyNode-Driven coding are presented in Section III-A, residual coding in Section III-B, and the Dual-direction prediction in Section III-C.

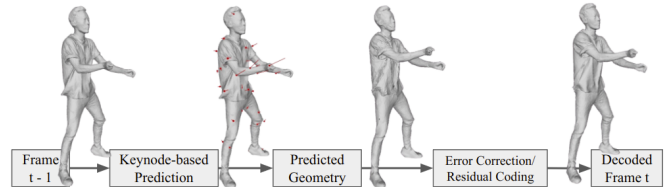


Fig. 1: Overall flow of the KeyNode-Driven approach.

A. KeyNode-Driven Geometry Coding

Consider a dynamic mesh $S = \{M_1, M_2, \dots, M_F\}$, where F represents the total number of frames in the sequence, and M_t denotes a static mesh at time t containing V_t vertices. The average number of vertices is denoted V . Static meshes in S may exhibit varying topologies.

Given two mesh frames M_{t-1} and M_t , an approximation of M_t , denoted M'_t , can be obtained through deforming M_{t-1} using an appropriate set of key nodes and their transformations. Let $\mathcal{GT}(\cdot)$ be a geometric transformation operator which deforms M_{t-1} to generate M'_t :

$$M'_t = \mathcal{GT}(M_{t-1}, \mathbf{n}, \mathbf{R}, \mathbf{T}) \quad (1)$$

Here, $\mathbf{n} = \{n_j \in \mathbb{R}^3\} \in \mathbb{R}^{N \times 3}$ is the set of key nodes, $\mathbf{R} = \{R_j \in \mathbb{R}^3\} \in \mathbb{R}^{N \times 3}$ and $\mathbf{T} = \{t_j \in \mathbb{R}^3\} \in \mathbb{R}^{N \times 3}$ are the key nodes’ affine transformations (rotations and translations), with $j \in [1, N]$ where $N \ll V$ is the total number of key nodes controlling the deformation of the mesh.

Each vertex x_i in M_{t-1} , $i \in [0, V_{t-1} - 1]$ is deformed according to its Q neighboring key nodes as:

$$x'_i = \mathcal{GT}(x_i) = \sum_{j=0}^{Q-1} w_{ij} (R_j(x_i - n_j) + t_j + n_j) \quad (2)$$

where n_j, R_j, t_j are the position, rotation and translation of key node j , respectively, and w_{ij} is the influence weight of key node n_j for vertex x_i based on the Euclidean distance between them. To effectively compress, we need to reduce the number of nodes in \mathbf{n} and also identify \mathbf{R} and \mathbf{T} that capture the deformation between M_{t-1} and M_t using these nodes. Fig. 2 illustrates the encoder structure. The *Optimal Key Node Generator*, discussed below, aims to find a sparse set of key nodes \mathbf{n} . The *Rotation and Translation Extractor* aims to find the optimal transformations \mathbf{R} and \mathbf{T} for those nodes.

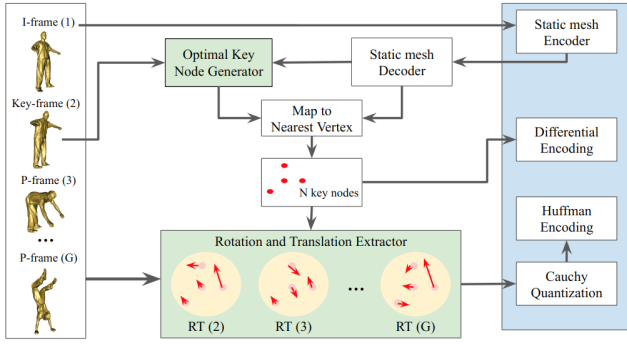


Fig. 2: Geometry encoder structure for a GoF with G frames.

Our geometry encoder divides a dynamic mesh into GoFs, each containing an initial I-frame followed by several P-frames. I-frames are encoded using V-DMC [21] all-Intra mode as a static mesh encoder as it consistently provided better performance than using Anchor for I-frame encoding.

To determine an appropriate set of key nodes, we consider the decoded I-frame to be the *source* and the subsequent P-frame (called the key-frame) to be the *target* in a source-target deformation pair. All P-frames, including key-frames, are transmitted using transformations of key nodes.

Key node placement impacts deformation quality. In [1], we presented an efficient optimization solution that balances compactness and quality by identifying the optimal set of key nodes. We formulated the balancing goal as a dual-objective optimization problem using the Alternating Direction Method of Multipliers (ADMM). To simplify the dual-objective formulation, a structured three-step approach (comprising a mesh registration model, coordinate descent, and gradient descent) is iteratively applied in a loop until the desired node sparsity is achieved. The *Optimal Key Node Generator* block in Fig. 2 employs that method, ensuring the set of chosen key nodes meets the target sparsity while minimizing distortion.

Once the optimal key nodes are identified, we map them to the decoded I-frame to find the closest vertex for each key node. These closest vertex positions are then adopted as the finalized positions of the key nodes, and will be used as n_j

in Eq. 2. We sort these vertex indexes in ascending order and encode them using differential encoding.

The optimal values for \mathbf{R} and \mathbf{T} are obtained through an optimization process in the *Rotation and Translation (RT) Extractor* module in Fig. 2, formulated as:

$$\underset{\mathbf{R}, \mathbf{T}}{\operatorname{argmin}} (\mathcal{L}_{data} + \alpha_{reg} \mathcal{L}_{reg} + \alpha_{rot} \mathcal{L}_{rot}) \quad (3)$$

Here, \mathcal{L}_{data} penalizes the geometry deviation between source and target; \mathcal{L}_{rot} measures the deviation of Rotation \mathbf{R} from the orthogonal matrix; and \mathcal{L}_{reg} ensures the smoothness of the deformation. We employ the approach introduced in [32] to solve this optimization problem.

For each P-frame, keynode transformations including $\mathbf{R} \in \mathbb{R}^{N \times 3}$ and $\mathbf{T} \in \mathbb{R}^{N \times 3}$ are flattened into a rotation vector and translation vector, denoted $\mathbf{R}^f \in \mathbb{R}^{3N}$ and $\mathbf{T}^f \in \mathbb{R}^{3N}$. Two Cauchy distributions are fitted to \mathbf{R}^f and \mathbf{T}^f . With a specified codebook size N_b^{RT} , N_b^{RT} equal-width bins are generated spanning from $-|b|$ to $|b|$, where b is the maximum absolute value within a given frame. The two middle bins are merged to create a dead-zone. The bin $(b_1^k, b_2^k]$ has its quantized value as the expected value of the Cauchy probability density function (pdf) within that range:

$$\Theta_k = \int_{b_1^k}^{b_2^k} \frac{x}{\pi\gamma(1 + (\frac{x-x_0}{\gamma})^2)} dx \quad (4)$$

where x_0, γ are the mean and variance of the fitted Cauchy distribution. Each transformation value l is quantized to the expected value of the range that it belongs to: $\hat{l} = \Theta_k$, if $b_1^k < l < b_2^k$.

A Huffman table is generated based on the probabilities; the probability of bin k with range $(b_1^k, b_2^k]$ is:

$$P_k = \int_{b_1^k}^{b_2^k} \frac{1}{\pi\gamma(1 + (\frac{x-x_0}{\gamma})^2)} dx \quad (5)$$

Hence, the overall transmission cost for each \mathbf{R}^f or \mathbf{T}^f contains the following components: mean and variance of the fitted Cauchy distribution, the border value $|b|$ for quantization bins, and the Huffman encoded bitstream.

At the decoder (Fig. 3), I-frames are decoded with the static mesh decoder. Given $\mathbf{n}, \mathbf{R}, \mathbf{T}$ retrieved through differential and Huffman decoding for P-frame M_t , its distorted mesh M'_t is reconstructed via deformation from M'_{t-1} , using Eq. 2.

B. Octree-based Geometric Residual Coding

Predicting P-frames using embedded key nodes introduces distortion, so we use a Geometric Residual Coding method based on octrees to reduce this geometric distortion.

1) *Spatial Octree-structured Residual Quantization*: Predicting P-frames through the transformation of embedded key nodes often means that areas of high motion or intricate detail exhibit larger residuals than those with slow and rigid motion. Let $M'_t = \{v'_0, v'_1, \dots, v'_{V_{IF}-1}\}$ denote the reconstructed mesh at time t , where v'_i represents the distorted position of vertex i , and V_{IF} is the number of vertices in M'_t (also in the I-frame associated with M_t). Let $\mathbf{r}_t = \{r_0, r_1, \dots, r_{V_{IF}-1}\}$ be

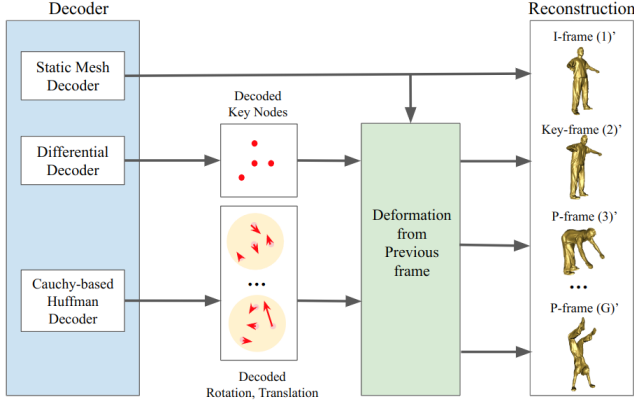


Fig. 3: Geometry Decoder structure for a GoF with G frames

the residual frame which represents the displacement of M'_t vertices relative to the source mesh M_t . To take advantage of the residual clustering effect, the *Spatial Partitioning* module (see Fig. 4) divides vertices in M'_t into octree cells based on their positions. The resulting octree contains L non-empty leaf nodes, $\mathcal{L} = \{l_0, l_1, \dots, l_{L-1}\}$, where leaf node l contains V_l vertices $\{v_0^l, v_1^l, \dots, v_{V_l-1}^l\} \subset M'_t$ that have residuals $\{r_0^l, r_1^l, \dots, r_{V_l-1}^l\}$, a subset of \mathbf{r}_t . In the *Residual Quantization* module, the quantized value \hat{r}^l for these residuals is computed as the average of the residuals belonging to non-empty leaf node l . Fig. 5 shows some residual frames quantized by different octrees. The system transmits the octree structure and \hat{r}^l for each leaf.

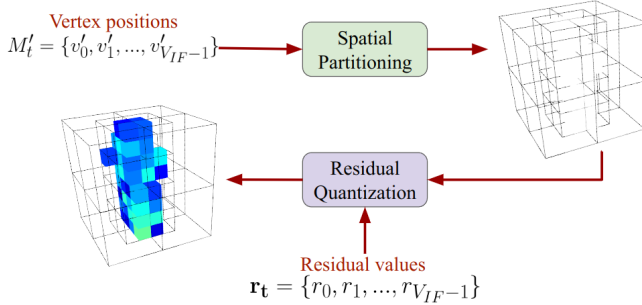


Fig. 4: Spatial octree-structured residual quantization method. Cell colors represent quantized residual values.

As P-frames are deformed from their I-frame and inherit the I-frame's topology, calculating prediction residuals is challenging since the reconstructed P-frames lack vertex correspondence with the source P-frames. A common technique to calculate \mathbf{r}_t is to compute the position difference between each distorted vertex and its closest vertex in the source mesh. However, if multiple distorted vertices share the same closest source vertex, perfect residual correction would lead them to all move to the same position in the corrected mesh. This issue, called duplicated vertices, can lead to undesired self-intersection of triangles in the corrected mesh. To avoid this, instead of mapping v'_i to the closest vertex in M_t , we identify the closest point on the surface of M_t , denoted v_i^* . The residual of a vertex i is then calculated as the positional difference

between v_i^* and v'_i :

$$r_i = v_i^* - v'_i \quad (6)$$

The mesh containing vertices $\{v_i^*\}$ and having M'_t 's topology is called the *approximate source mesh* for M'_t .

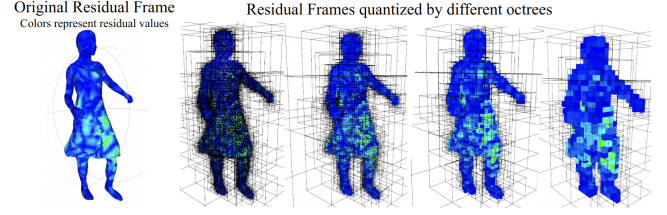


Fig. 5: Visualizations of a residual frame being quantized by different octrees, resulting in different levels of detail.

2) *Cost-constrained Octree Generation*: Determining a suitable octree structure to efficiently quantize the residuals is crucial. In this section, we present a cost-constrained approach for generating a suitable unbalanced octree for each residual frame, balancing residual distortion and octree size (bitrate) through a cost function of an optimization problem. When a residual frame \mathbf{r}_t is quantized by an octree T , we denote the quantized frame by $\hat{\mathbf{r}}_t = \{\hat{r}_0, \hat{r}_1, \dots, \hat{r}_{V_{IF}-1}\}$, where each \hat{r}_i represents the average residual of the leaf node to which r_i belongs. The overall quantization distortion can be calculated as the mean squared error between the original and quantized residual frames:

$$D(T) = MSE(\mathbf{r}_t, \hat{\mathbf{r}}_t). \quad (7)$$

Let $c(T)$ be the cost of octree T ; we link $c(T)$ to the number of leaf nodes, since the size of T directly affects the bitrate. Given a cost constraint c , the octree with minimized distortion is called the optimal tree for constraint c :

$$T_{opt} = \operatorname{argmin} D(T) \quad (8)$$

such that $c(T) \leq c$. To identify T_{opt} , we compute a 'quality factor' λ for each node n based on the ratio of the change in distortion to the change in cost from expanding node n :

$$\lambda(n) = \frac{\Delta D(n)}{\Delta C(n)} = \frac{D(T) - D(T(n))}{C(T(n)) - C(T)} \quad (9)$$

Here, $D(T)$ is the distortion of the octree T in which n is a leaf node, $D(T(n))$ is the distortion of the octree in which n is expanded, and $\lambda(n)$ is the slope of the cost-distortion curve when adjusting the octree structure.

When growing the octree, the node with the largest $\lambda(n)$ will be chosen to expand, and when pruning, the node with the smallest $\lambda(n)$ will be made a leaf.

To avoid calculating the distortion and cost for the whole tree, we compute $\lambda(n)$ based on the distortion of the node being evaluated [33]:

$$\Delta D(n) = D(n) - \sum_{i=0}^7 \frac{p(n_i)}{p(n)} D(n_i) \quad (10)$$

Here, $n_i, 0 \leq i \leq 7$, are the possible children of node n , $p(n) = \frac{V_n}{V_{IF}}$, where V_n is the number of vertices in node n

and $D(n)$ is the distortion between the original and quantized residuals in node n :

$$D(n) = MSE\left(\{r_0^n, r_1^n, \dots, r_{V_n-1}^n\}, \{\hat{r}^n, \hat{r}^n, \dots, \hat{r}^n\}\right) \quad (11)$$

where \hat{r}^n is the quantized residual value for node n .

3) *Coding of Octree-based Quantized Residuals*: Fig. 6 depicts the structure for residual coding. At the encoder, the distorted P-frame M_t^l is used to generate a balanced octree based on the vertex positions. When vertices are accurately predicted through deformation, they should not be corrected with residual coding. To determine which nodes should carry residuals, we compare the average vertex distortion e^l of the node's vertices with a threshold \mathcal{T} . In our implementation, the value of e^l is derived from the Mesh Structural Distortion Measure ver. 2 (MSDM2) [34] distortion metric, while it could also be directly calculated as \hat{r}^l to save computational cost. All nodes where $e^l < \mathcal{T}$ are referred to as Non-Correcting Octree Cells (NCOC); residuals for their vertices will not be transmitted. Non-correcting flags are sent only for the highest-level NCOC parents, as their children inherit the same type. The octree is then pruned using the cost-constrained method. Pruning flags are sent to the decoder, allowing it to reconstruct the unbalanced octree.

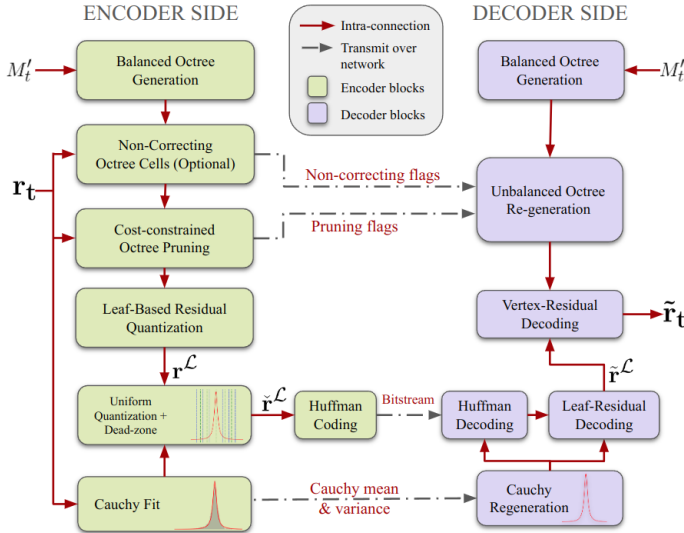


Fig. 6: Codec structure for Residual coding.

The residuals are quantized with the unbalanced octree, and then each dimension of $\mathbf{r}^{\mathcal{L}}$ undergoes uniform quantization with a dead-zone. A Cauchy distribution is fitted to the original residual frame \mathbf{r}_t in the corresponding dimension, which is used to construct the Huffman codebook in a manner similar to the process described in Eqs. 4 and 5. This process is repeated for each dimension independently. Overall, transmitting the residual frame \mathbf{r}_t requires: two binary streams of flags, three bitstreams of Huffman-coded leaf residuals, and three fitted Cauchy distributions described by their means and variances.

To decode the residual frame \mathbf{r}_t , the unbalanced octree is constructed using the distorted P-frame M_t^l and the received flags. Leaf residuals $\tilde{\mathbf{r}}^{\mathcal{L}}$ are obtained by decoding bitstreams using the Huffman codebook constructed through the received

Cauchy distributions. The decoded vertex residual $\tilde{r}_i \in \tilde{\mathbf{r}}_t$ is calculated as the value of the quantized residual of its associated leaf.

C. Dual-direction Prediction

In our codec, P-frames are predicted from either an I-frame or another P-frame. Distortion can accumulate across frames, and later P-frames typically have higher distortion than earlier ones. Dual-direction Prediction (Fig. 7) predicts P-frames from both directions. A *switch index* determines when the prediction direction changes.

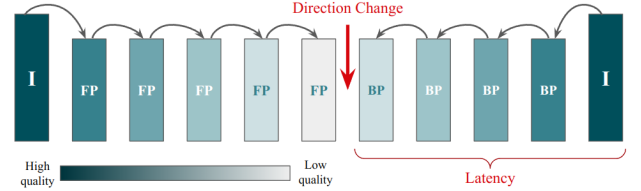


Fig. 7: Dual-direction Prediction flow, where P-frames are predicted from both directions. Labels: **I** for I-frames, **FP** for Forward P-frames, and **BP** for Backward P-frames.

If the switch index is predetermined and fixed, the prediction direction is based solely on temporal distance from the reference frame, ensuring minimal complexity. This results in a fixed number of backward P-frames, and the latency is equal to this number.

When the switch index is determined adaptively, the codec evaluates prediction quality in both forward and backward directions for each P-frame to identify the optimal switching point. In this mode, temporal distance alone does not dictate the prediction direction; instead, quality considerations drive the choice. Adaptive switching increases latency to the size of the GoF and requires additional encoder storage to hold frames predicted from both directions until the switch index is finalized.

The selection of fixed or adaptive direction switching depends on the application, especially concerning latency and encoder storage capacity.

IV. EVALUATION

A. Datasets and Metrics

To thoroughly evaluate the performance of our KeyNode-driven codec, we conducted experiments on a diverse set of scanned dynamic mesh sequences, each chosen to highlight different challenges and characteristics. Details about the mesh sequences are in Table I. We categorize the sequences into three groups. In the *Slow Motion* category, consecutive frames usually have significant overlap. In the *Fast Motion* category, consecutive frames often exhibit noticeable changes in the position or orientation of body part(s) and/or rapid movement of clothing. *Join/Split* contains a mesh sequence with dynamic interactions between two objects (a person and a ball) that connect and disconnect across frames.

In this article, we use MSDM2 [34] for geometry distortion evaluation due to its proven high correlation with human

TABLE I: Statistics of the evaluated datasets.

Category	Sequence	First Frame	Last Frame	Avg. # Vertices	Avg. # Faces	Capture Artifacts
Slow Motion	Mitch	1	300	16676	30000	
	Soldier	536	835	22702	39989	Holes
	Thomas	618	917	16235	30000	
Fast Motion	Longdress	1051	1350	22231	39991	Outliers & holes
	Dancer	1	300	20908	39373	Holes
	Levi	0	149	47580	39984	Holes
Join/Split	Basketball	1	300	20903	39456	Outliers & holes

visual perception through extensive subjective experiments. MSDM2 measures local curvature differences between two meshes, providing a distortion score in the range [0,1], where 0 indicates identical meshes, and values approaching 1 signify substantial visual dissimilarity. Since MSDM2 is designed for static meshes, to determine the overall sequence distortion, the average value across frames is calculated.

B. KeyNode-based Compression Hyper-parameters

The number N_b^{res} of quantization levels for residuals is set to 128 for all sequences, and N_b^{RT} for key node rotations and translations is set to 64. NCOC mode is used only for *Soldier*, *Thomas*, and *Mitch* because of their sufficiently accurate P-frame prediction. We assigned 100 key nodes to *Soldier*, *Thomas*, and *Levi*, 200 to *Mitch*, and 300 to *Longdress*, *Basketball*, and *Dancer*. More key nodes are assigned to sequences with more complex motion to enhance P-frame prediction.

We evaluate two variants of our KeyNode-based method: *Fully Forward (FF)*, where each P-frame is predicted from its preceding frame, and *Adaptive Dual-direction Prediction (ADP)*, where the change in direction depends on the prediction quality from both directions, leading to a latency equal to the GoF size.

C. Analysis of KeyNode-based Encoded Components

This section offers a closer examination of our codec elements. For a dynamic mesh, we transmit the statically encoded I-frames, encoded key nodes, encoded RT, and encoded residuals for P-frames. Figs. 8 and 9 illustrate the proportion of each encoded component as the GoF size and number of key nodes vary. The proportion of encoded residuals increases the most with GoF size increases; this is due to a smaller number of I-frames for large GoF cases. When the number of key nodes increases, the encoded RT component increases proportionally, while the geometry residual proportion decreases, because a larger number of key nodes does better P-frame prediction, leading to lower prediction errors.

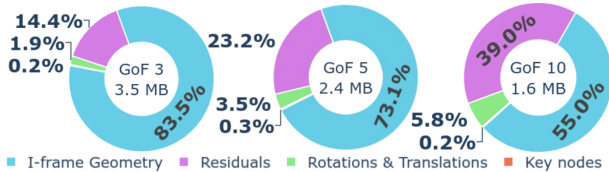


Fig. 8: Encoded components when varying GoF size in *Thomas*. The number of key nodes is 100.

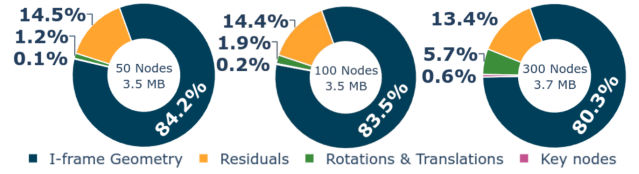


Fig. 9: Encoded components when varying number of key nodes in *Thomas*. GoF size is 3 frames.

D. Distributions of Encoding parameters

In our codec, RT and residuals are quantized and Huffman-coded with a fitted Cauchy distribution. Fig. 10 presents the distributions of our data with the fitted Gaussian, Laplace, and Cauchy distributions. The Cauchy distribution has the best alignment with the data. Y-axis and Z-axis residuals have a similar histogram with the X-axis in Fig. 10a, and key node translations have a similar histogram with Fig. 10b.

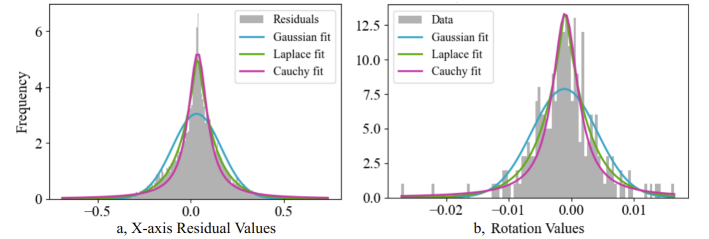


Fig. 10: Distributions of Residuals and RT in frame 618 of *Thomas*. The histograms are plotted with 200 bins.

E. Geometry Errors at each Compression Stage

Fig. 11 shows the geometric distortion at each compression phase of our method, specifically: the predicted P-frame prior to residual coding (b), the approximate source mesh for that frame (c), and the corrected mesh post-residual coding (d).

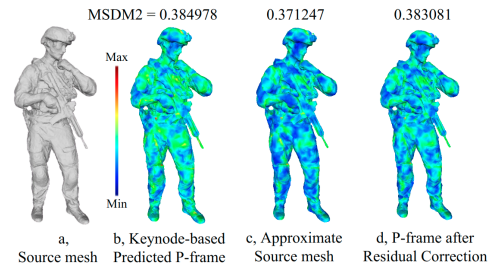


Fig. 11: MSDM2 Distortion at each stage of compressing frame 537 in *Soldier* as the first P-frame in a GoF.

In Fig. 11b, the frame predicted based on key nodes shows some degree of distortion, which is then reduced with residual coding, as seen in Fig. 11d. The approximate source mesh in Fig. 11c serves as a reference for the residual calculation. In essence, if the residuals could be compressed losslessly, Fig. 11c would represent the best-corrected frame.

F. Influence of GoF Size and I-frame Quality

In this section, we evaluate various GoF sizes and I-frame qualities to understand how they impact compression performance. The experiment is done on *Thomas's* first ten frames, with four different GoF sizes and four different I-frame quality levels. We evaluate the I-frame quality levels 1 to 4 from lower to higher. For P-frames, we use the same encoding configuration across all cases being assessed.

Fig. 12 shows that smaller GoF sizes are more sensitive to variations in I-frame quality, as indicated by a wider spread in compression performance when changing quality levels. Smaller GoF sizes lead to higher bit rates, whereas larger GoF sizes tend to perform better at lower bit rates. For instance, at similar quality settings, GoF size 10 achieves a lower bit rate. Overall, Fig. 12 suggests that the KeyNode-based method prefers medium to high I-frame quality. When aiming for lower target bit rates, it is advantageous to increase the GoF size rather than reduce the quality of the I-frames.

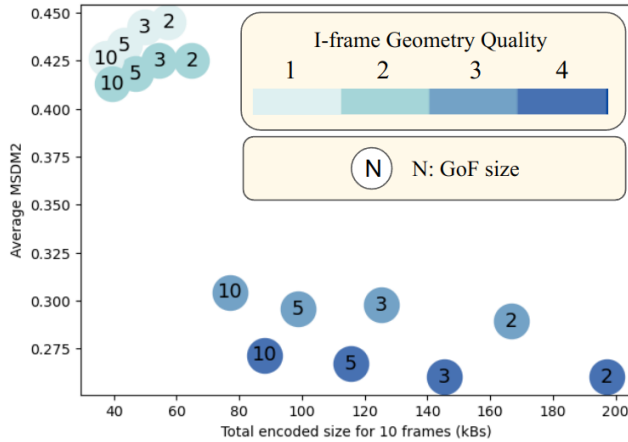


Fig. 12: Influence of GoF size and I-frame quality on compression performance - first ten frames in *Thomas* sequence.

Additionally, it can be noticed that when the I-frame geometry quality is low (e.g., 1 and 2), increasing the GoF size slightly reduces distortion. This occurs because the octree-based residual coding effectively enhances the quality of P-frames, causing P-frames to have slightly lower distortion than I-frames.

G. Influence of P-frame Encoding Components

P-frames are predicted and encoded using the key nodes and their transformations RT, as well as the geometric residuals. The values chosen for each component affect the compression performance. To assess sensitivity to variations in parameters, we examine performance across many parameter sets in Fig. 13.

It is evident that the octree size for residual coding significantly impacts the rate, as the squares are predominantly on the right side, while the circles are clustered on the left. With a notable increase in rate, enlarging the octree usually leads to an improvement in quality, as the residuals are described more accurately with bigger octrees.

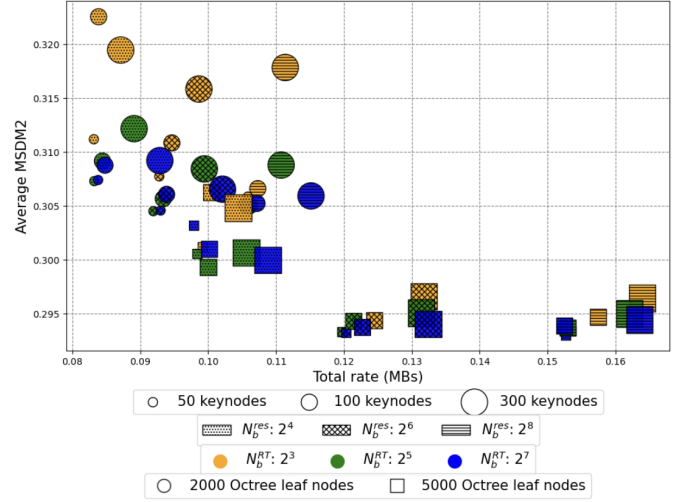


Fig. 13: Influence of P-frame compression parameters for the first ten frames of *Basketball* with GoF size = 5.

In Fig. 13, similar hatch patterns tend to form distinct vertical clusters, suggesting that N_b^{res} strongly influences the rate.

Unlike the octree size and N_b^{res} , varying N_b^{RT} does not strongly impact the rate. However, those parameters primarily control the quality when the other two parameters are fixed.

Additionally, each value of N_b^{RT} can cover the entire range on the rate axis, but the green and blue markers generally achieve lower distortion values with only a small increase in rate. Consequently, it appears desirable to use larger values of N_b^{RT} .

H. Compression Performance Comparison

In this section, we compare the Rate-Distortion (RD) performance of our KeyNode-based method with the state-of-the-art V-DMC's geometry coding method [21] with their two modes: all intra-coding (denoted by *V-DMC - intra*), and with inter coding frames (denoted by *V-DMC - inter*). V-DMC was chosen as the baseline because it demonstrated the highest effectiveness among methods responding to the MPEG call for proposals and offers a publicly available implementation, enabling fair and reproducible comparisons.

For Slow Motion sequences, Fig. 14 presents the RD curves using the MSDM2 metric. The results show that our method outperforms V-DMC considerably on these sequences, especially at low bitrates.

For the Fast Motion and Join/Split categories, Fig. 15 depicts the RD curves using MSDM2. Our methods are slightly better than V-DMC on the *Longdress*, *Levi*, and *Basketball* sequences and slightly worse on *Dancer*.

The *Basketball* sequence involves different objects joining and separating over time. Since our method uses a fixed size for the GoF throughout the sequence, our prediction model may encounter challenges when objects join and separate. The compression performance might be improved by incorporating an adaptive GoF scheme, allowing for the dynamic insertion of I-frames as needed.

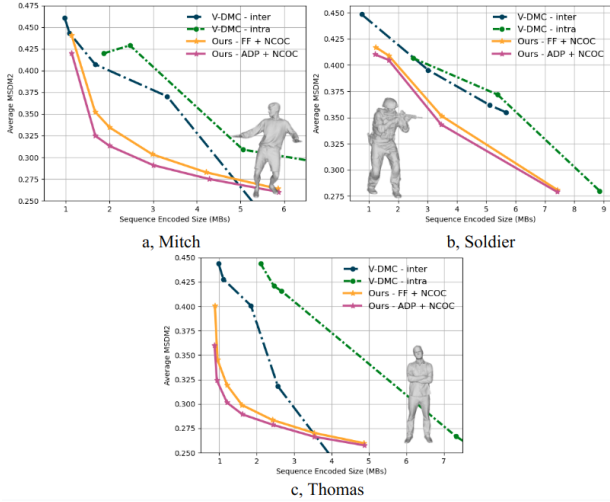


Fig. 14: Geometric distortion comparison of methods on Slow Motion sequences.

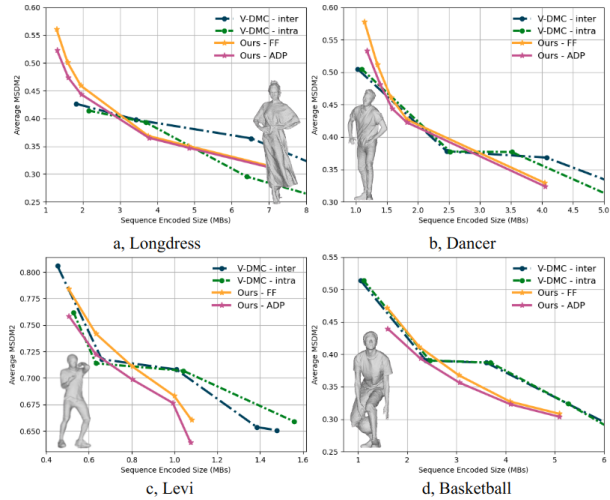


Fig. 15: Geometric distortion comparison on Fast Motion and Join/Split categories.

The curves in Figures 14 and 15 can be summarized in terms of average bitrate savings using Bjøntegaard Delta rate (BD-rate) percentage, following the methodology in [35]. Table II presents the BD-rate percentages compared to two coding modes of V-DMC. BD-rate measures the difference in bit rate required to achieve the same level of distortion between two compression methods. A lower BD-rate indicates better compression efficiency, as it achieves the same quality with less data. Consequently, in Table II, negative values indicate that Ours outperforms the comparison method, while positive values indicate that Ours performs worse. According to Table II, our methods considerably outperform V-DMC for sequences in the Slow Motion Category. For sequences in the Fast Motion category, compared to V-DMC, our methods perform slightly better on *Longdress*, slightly worse on *Dancer*, and comparably on *Levi*. For the Join/Split category, we outperform V-DMC by a small margin.

TABLE II: BD-rate (%) of Ours against V-DMC.

		Slow Motion			Fast Motion			Join/Split	Avg.
		Soldier	Thomas	Mitch	Longdress	Dancer	Levi	Basketball	
V-DMC	FF	-32.58	-46.12	-37.57	-23.05	9.61	0.12	-1.90	-18.78
	ADP	-37.14	-48.70	-48.99	-26.06	4.61	-13.45	-19.07	-26.97
V-DMC	FF	-36.71	-76.45	-41.78	-3.92	9.39	-5.70	-1.85	-22.43
	ADP	-40.45	-79.95	-50.91	-6.92	4.54	-17.56	-17.74	-29.86
Average									-24.51

I. Frame-wise and GoF-wise Distortion Analysis

Fig. 16 provides frame-wise and GoF-wise distortion for different methods at a similar encoded size. In Fig. 16a, among our KeyNode-based coded frames in both FF and ADP modes, the I-frames exhibit the smallest errors, as they are encoded with high quality using a static mesh encoder. As seen in Fig. 16b, our FF mode typically exceeds V-DMC's performance across most GoFs, although there is one GoF in the middle of the sequence where it performs worse than V-DMC's inter-coding. However, our ADP mode manages this GoF effectively.

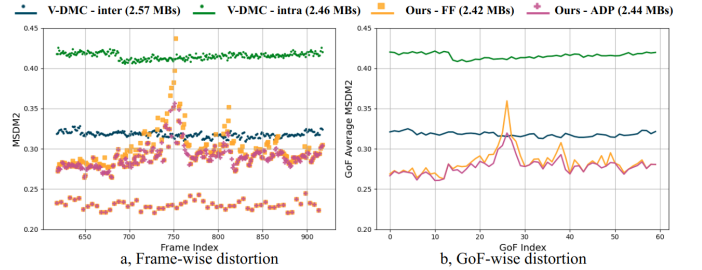


Fig. 16: Frame-wise (a) and GoF-wise (b) analysis for *Thomas* under similar sequence encoded size. The evaluated GoF size is 5 frames. *Label format: Method (Sequence encoded size)*.

To examine that specific GoF more closely, Fig. 17 displays the frames within this GoF encoded using different modes. In the source mesh, frames 738 and 739 show the left arm attached to the body, while frames 740 to 743 depict the arm gradually detaching from the body, indicating a topological change. It is clear that forward prediction struggles to capture the arm's detachment accurately. In contrast, the third row, which uses backward prediction, shows that frames 740, 741, and 742 are accurately predicted from I-frame 743, as they preserve a similar topology. With Dual-direction Prediction, which leverages both prediction directions, P-frames within the GoF can be predicted more accurately using I-frames with a similar, though not necessarily identical, topological structure. The visualizations effectively demonstrate how ADP mode reduces distortion in this GoF.

Besides the example in Fig. 17, where it is advantageous to switch to backward prediction at a frame that is not the middle of the GoF, Fig. 18 shows additional examples to demonstrate the benefits of an adaptive scheme for direction switching, since backward prediction could perform better not only in the middle of the GoF but also near its beginning or end.

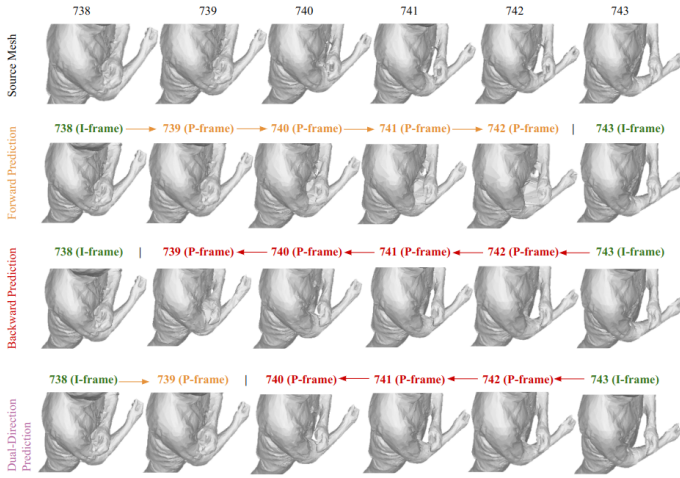


Fig. 17: Decoded meshes illustrate the topological change issue in *Thomas*, managed by Dual-direction prediction.

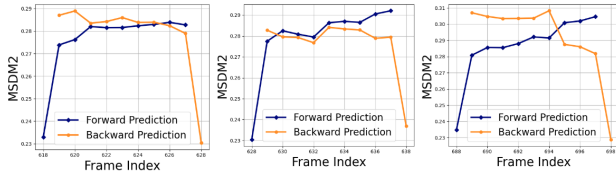


Fig. 18: Frame-wise MSDM2 from two prediction directions in three GoFs, where the ideal direction change index is not in the middle of the GoF, highlighting the preference for an adaptive scheme.

J. Geometry Reconstruction Distortion

Fig. 19 provides a visual comparison between the reconstruction errors of our compression approach and V-DMC under similar bitrate for the *Thomas* sequence. The meshes are colored based on MSDM2 distortion, indicating the accuracy of geometry reconstruction. Warmer colors (reds) indicate higher reconstruction errors, while cooler colors suggest areas where the reconstruction closely matches the original mesh.

Notably, with *Thomas* in Fig. 19, our method achieves lower errors with a similar bitrate. In the zoom-in region, our decoded mesh more closely resembles the original mesh than that of V-DMC, which tends to lose the details of the fingers.

Similarly, Fig. 20 provides a visual comparison of a frame extracted from decoded *Levi* sequences. The total sequence encoded bitrate and average MSDM2 are listed alongside each method. Fig. 20 shows that for that decoded frame, our method preserves details more effectively than V-DMC. This is particularly noticeable when zooming in on the model’s head, where our decoded mesh maintains the shape of the nose and lips more accurately.

V. DISCUSSION AND FUTURE WORK

In this paper, we introduce an efficient approach to compress real-world scanned 3D dynamic human meshes by leveraging embedded key nodes and their transformations to capture the temporal evolution of vertices. We proposed a

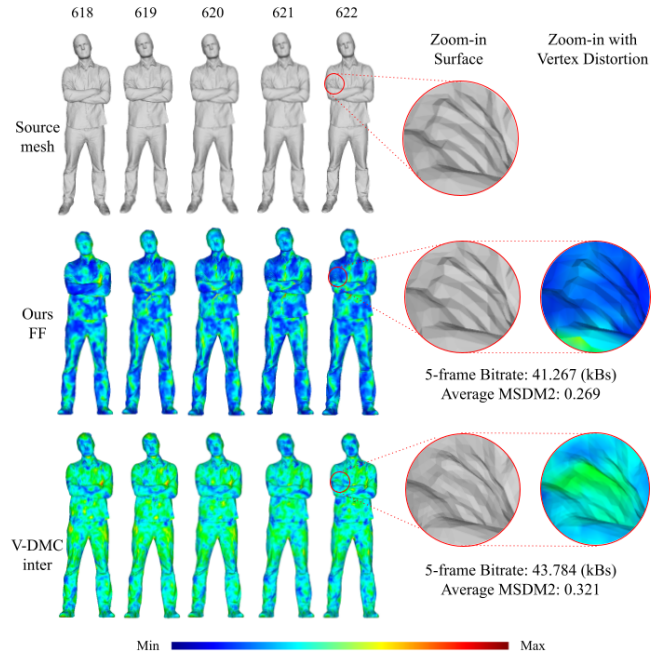


Fig. 19: Reconstruction distortion of our method and V-DMC, under similar bitrate, for frames 618 to 622 in *Thomas*. The first mesh in Ours is an I-frame, and the four other meshes are forward P-frames.

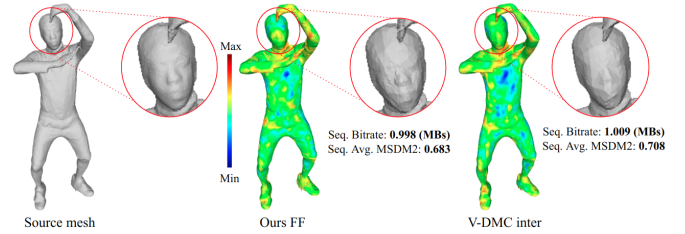


Fig. 20: Frame 13 of *levi*, extracted from the decoded sequences using our method and V-DMC.

strategy where the temporal change of each vertex is computed as a weighted combination of key node transformations, facilitating a comprehensive representation of motion. Our KeyNode-driven method addresses the challenges of dynamic human mesh compression by effectively handling topology changes between frames and accommodating scan imperfections. Through the use of sparse key nodes, our approach accurately captures and represents the complexities of human motion, achieving efficient compression. To enhance the quality of the KeyNode-based prediction, we present an octree-based residual coding scheme and a Dual-direction prediction mode to further improve temporal prediction.

Our method presents notable advantages in geometry coding compared to V-DMC, particularly evident in the Slow Motion sequence category. For Fast Motion and Join/Split sequences, our approach demonstrates comparable performance. These results highlight the effectiveness of our method in handling varying topology and scan defects, while also emphasizing the challenge of accurately predicting the geometry of P-frames

in human dynamic meshes with rapid motions.

Our KeyNode-driven codec introduces a new way to compress scanned 3D human dynamic models, opening up numerous avenues for future research and development. One promising direction is the adaptive placement of I-frames, where dynamically determining the optimal points for I-frame insertion could further enhance compression performance. Another potential improvement is the integration of view-dependent coding, which takes into account that users typically view a 3D model from a single angle at a time. By reducing the quality of unseen areas, we can lower bitrate requirements without compromising the user experience. Additionally, while the current KeyNode-driven codec delivers effective results, its encoding complexity remains a limitation. The optimization-based nature of components such as the *Optimal Key Node Generator* and *Rotation and Translation Extractor* can be computationally demanding. Future work could focus on relaxing these optimization steps and exploring parallelization techniques to improve efficiency. Furthermore, the KeyNode-driven codec holds great potential for broader applicability by adapting the prediction model to align with the characteristics of diverse mesh structures. While the current method is optimized for objects exhibiting a combination of rigid and non-rigid motions, such as dynamic human meshes, future work could explore alternative transformation prediction strategies or tailored strategies for different types, unlocking its versatility across a range of scanned models.

REFERENCES

- [1] H. Hoang, K. Chen, T. Nguyen, and P. Cosman, "Embedded Deformation-based Compression for Human 3D Dynamic Meshes with Changing Topology," in *IEEE/CVF Int. Conf. Comput. Vision Workshops*, 2023, pp. 2244–2254.
- [2] C. L. Bajaj, V. Pascucci, and G. Zhuang, "Single resolution compression of arbitrary triangular meshes with properties," ser. DCC '99. USA: IEEE Computer Society, 1999, p. 247.
- [3] S. Gupta, K. Sengupta, and A. A. Kassim, "Compression of Dynamic 3D Geometry Data Using Iterative Closest Point Algorithm," vol. 87, no. 1–3, p. 116–130, jul 2002.
- [4] N. Stefanoski and J. Ostermann, "SPC: Fast and Efficient Scalable Predictive Coding of Animated Meshes," *Comput. Graph. Forum*, vol. 29, no. 1, pp. 101–116, 2010.
- [5] M. O. Bici and G. B. Akar, "Improved prediction methods for scalable predictive animated mesh compression," *J. Vis. Commun. Image Rep.*, vol. 22, no. 7, pp. 577–589, 2011.
- [6] J.-K. Ahn, Y. J. Koh, and C.-S. Kim, "Efficient Fine-Granular Scalable Coding of 3D Mesh Sequences," *IEEE Trans. Multimedia*, vol. 15, no. 3, pp. 485–497, 2013.
- [7] M. Alexa and W. Muller, "Representing Animations by Principal Components," *Comput. Graph. Forum*, 2000.
- [8] Z. Karni and C. Gotsman, "Compression of soft-body animation sequences," *Computers & Graphics*, vol. 28, no. 1, pp. 25–34, Feb. 2004.
- [9] A. S. Lalos, G. Arvanitis, A. Spathis-Papadiotis, and K. Moustakas, "Feature Aware 3D Mesh Compression Using Robust Principal Component Analysis," in *IEEE Int. Conf. Multimedia Expo*, 2018, pp. 1–6.
- [10] M. Sattler, R. Sarlette, and R. Klein, "Simple and efficient compression of animation sequences," in *Proc. 2005 ACM SIGGRAPH/Eurographics Symp. Comput. Anim.*, ser. SCA '05. New York, NY, USA: Association for Computing Machinery, 2005, p. 209–217.
- [11] I. Guskov and A. Khodakovsky, "Wavelet Compression of Parametrically Coherent Mesh Sequences," in *Proc. ACM SIGGRAPH/Eurographics Symp. Comput. Anim.*, ser. SCA '04. Goslar, DEU: Eurographics Association, 2004, p. 183–192.
- [12] F. Payan and M. Antonini, "Temporal wavelet-based compression for 3D animated models," *Computers & Graphics*, vol. 31, no. 1, pp. 77–88, Jan. 2007.
- [13] J.-H. Yang, C.-S. Kim, and S.-U. Lee, "Progressive coding of 3D dynamic mesh sequences using spatiotemporal decomposition," in *IEEE Int. Symp. Circuits Syst.*, 2005, pp. 944–947 Vol. 2.
- [14] A. Collet, M. Chuang, P. Sweeney, D. Gillett, D. Evseev, D. Calabrese, H. Hoppe, A. Kirk, and S. Sullivan, "High-Quality Streamable Free-Viewpoint Video," *ACM Trans. Graph.*, vol. 34, no. 4, jul 2015.
- [15] S.-R. Han, T. Yamasaki, and K. Aizawa, "Time-Varying Mesh Compression Using an Extended Block Matching Algorithm," *IEEE Trans. on Circuits & Syst. for Video Tech.*, vol. 17, no. 11, pp. 1506–1518, 2007.
- [16] T. Yamasaki and K. Aizawa, "Patch-based compression for Time-Varying Meshes," in *IEEE Int. Conf. Image Process.*, 2010, pp. 3433–3436.
- [17] D. B. Graziosi, "Video-Based Dynamic Mesh Coding," in *IEEE Int. Conf. Image Process.*, 2021, pp. 3133–3137.
- [18] "CfP for Dynamic Mesh Coding," *ISO/IEC JTC1/SC29/WG7/N00231*, Oct. 2021.
- [19] Draco: 3D Data Compression. <https://github.com/google/draco>. [Online]. Available: <https://github.com/google/draco>
- [20] J.-E. Marvie, M. Krivokuća, C. Guede, J. Ricard, O. Mocquard, and F.-L. Tariolle, "Compression of Time-Varying Textured Meshes using Patch Tiling and Image-based Tracking," in *Eur. Workshop Vis. Info. Process.*, 2022, pp. 1–6.
- [21] K. Mammou, J. Kim, A. M. Tourapis, D. Podborski, and D. Flynn, "Video and Subdivision based Mesh Coding," in *Eur. Workshop Vis. Info. Process.*, 2022, pp. 1–6.
- [22] H. Nishimura, H. Kato, and K. Kawamura, "Hierarchical arithmetic coding of displacements for dynamic mesh compression," in *IEEE Int. Conf. Image Process.*, 2023, pp. 2850–2854.
- [23] X. Jin, J. Xu, and K. Kawamura, "Embedded graph representation for inter-frame coding of dynamic meshes," in *ICASSP 2024 - 2024 IEEE International Conference on Acoustics, Speech and Signal Processing (ICASSP)*, 2024, pp. 4070–4074.
- [24] H. Nishimura, H. Kato, and K. Kawamura, "Arithmetic Coding of Displacements in Dynamic Meshes with Bypass Mode for Complexity Reduction," in *IEEE Int. Conf. Vis. Comm. Image Process.*, 2023, pp. 1–5.
- [25] A. Martemianov and P. R. Alface, "Lossy video coding of v-dmc displacements," in *2024 Picture Coding Symposium (PCS)*, 2024, pp. 1–5.
- [26] P. R. Alface, D. Nam, L. Kondrad, and S. Y. Lim, "Level-of-detail adaptive subdivision methods for the coding of dynamic mesh sequences with v-dmc," in *2024 12th European Workshop on Visual Information Processing (EUVIP)*, 2024, pp. 1–6.
- [27] P. R. Alface, L. Kondrad, and K. Kammachi-Sreedhar, "Enabling progressive dynamic mesh geometry data extraction in v-dmc," in *2024 12th European Workshop on Visual Information Processing (EUVIP)*, 2024, pp. 1–6.
- [28] K. Kishimoto, K. Kawamura, and H. Kato, "Minimization of submesh boundary errors in dynamic mesh coding," in *2024 IEEE International Conference on Image Processing (ICIP)*, 2024, pp. 3368–3374.
- [29] X. Jin, J. Xu, and K. Kawamura, "Partial inter-frame coding for dynamic meshes," in *2024 IEEE International Conference on Image Processing (ICIP)*, 2024, pp. 3457–3463.
- [30] J. Xu, H. Kato, and K. Kawamura, "Temporal scalable coding for dynamic meshes," in *2024 IEEE International Conference on Image Processing (ICIP)*, 2024, pp. 3285–3291.
- [31] H. Nishimura, H. Kato, and K. Kawamura, "Quantization after inter prediction in displacement coding of dynamic meshes," in *2024 IEEE International Conference on Image Processing (ICIP)*, 2024, pp. 3361–3367.
- [32] K. Chen, F. Yin, B. Du, B. Wu, and T. Q. Nguyen, "Efficient Registration for Human Surfaces Via Isometric Regularization on Embedded Deformation," *IEEE Trans. Vis. Comput. Graphics*, pp. 1–13, 2022.
- [33] J. Lin and J. A. Storer, "Design and performance of tree-structured vector quantizers," *Info. Process. Manage.*, vol. 30, no. 6, p. 851–862, Nov. 1994.
- [34] G. Lavoué, "A Multiscale Metric for 3D Mesh Visual Quality Assessment," *Comput. Graph. Forum*, vol. 30, no. 5, pp. 1427–1437, Aug. 2011.
- [35] G. Bjøntegaard, "Calculation of Average PSNR Differences between RD-curves," in *VCEG-M33*, 2001.